THE JOURNAL OF PHYSICAL CHEMISTRY C

Article

pubs.acs.org/JPCC

Predicting Solar-Cell Dyes for Cosensitization

Sam L. Bayliss,[†] Jacqueline M. Cole,*[,†,‡,∥] Paul G. Waddell,[†,§] Scott McKechnie,[†] and Xiaogang Liu[†]

[†]Cavendish Laboratory, Department of Physics, University of Cambridge, J. J. Thomson Avenue, Cambridge, CB3 0HE, United Kingdom

[‡]Argonne National Laboratory, 9700 South Cass Avenue, Argonne, Illinois 60439, United States

[§]Australian Nuclear Science and Technology Organization, Lucas Heights, New South Wales 2234, Australia

[∥]Institute For Complex Adaptive Matter, University of California, Davis, California 95616, United States

Supporting Information

ABSTRACT: A major limitation of using organic dyes for dye-sensitized solar cells (DSCs) has been their lack of broad optical absorption. Cosensitization, in which two complementary dyes are incorporated into a DSC, offers a route to combat this problem. Here we construct and implement a design route for materials discovery of new dyes for cosensitization, beginning with a chemically compatible series of existing laser dyes which are without an anchor group necessary for DSC use. We determine the crystal structures for this dye series and use their geometries to establish the DSC molecular design prerequisites aided by density-functional theory and time-dependent density-functional theory calculations. Based on insights gained from these existing dyes, modified sensitizers are computationally designed to include a suitable anchor group. A DSC cosensitization strategy for these modified sensitizers is predicted, using the central features of highest-occupied and lowest-unoccupied molecular orbital positioning, optical absorption properties, intramolecular charge-transfer characteristics, and steric effects as selection criteria. Through this molecular engineering of a series of existing non-DSC dyes, we predict new materials for DSC cosensitization.

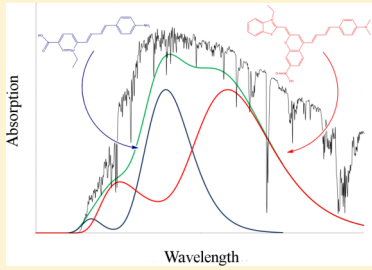

INTRODUCTION

Dye-sensitized solar cells are a promising candidate for next-generation photovoltaics.[1] Of central importance to their operation is the light-absorbing dye which is anchored to a semiconductor, typically TiO_2. On photoexcitation, the dye injects an electron into the semiconductor conduction band, which is then regenerated by electron donation from an electrolyte, typically the iodide/triiodide redox couple. So far, DSCs containing the ruthenium-based *N719* dyes have produced some of the highest power-conversion efficiencies,[1] but organic chromophores are attractive alternative dyes due to their lower cost, higher extinction coefficients, and tunable optical properties. However, their narrow absorption bands have proven problematic as this limits the harnessing of the broad-band solar spectrum.[2] Cosensitization is a promising remedy to obtain broad spectral coverage, but a systematic means of predicting efficient dye combinations for this application is needed.[3]

Most successful organic dyes are based on the D-π-A, or push−pull, architecture, in which an electron donor, D, is linked through a π-conjugated bridge to an acceptor, A, which is connected to the semiconductor through an anchor group, such as a carboxylic acid. The key criteria for dye cosensitizer selection are (i) a lowest unoccupied molecular orbital (LUMO) energy level that lies above the semiconductor conduction band, (ii) a highest occupied molecular orbital (HOMO) energy level that lies below the electrolyte redox potential, (iii) the presence of an anchor group to provide the coupling between dye and semiconductor, (iv) directed intramolecular charge transfer on photoexcitation from donor to semiconductor via the anchor, (v) chemical compatibility between dye cosensitizers, and (vi) a high molecular extinction coefficient: this is key for cosensitization in allowing attachment of multiple dyes, while minimizing their mutual interactions.[4]

With high molecular extinction coefficients, tunable absorption spectra, and good optical excitation cycling efficiencies, organic laser dyes are an attractive basis for designing new DSC sensitizers. Here we use a series of chemically similar, and therefore mutually compatible, organic laser dyes **1**−**7** (Figure 1) as the starting point for molecular engineering of organic chromophores for cosensitization. These dyes do not contain an anchor group necessary for DSC use, but we use them as a basis to design new dyes with suitable anchoring groups, whose optical properties can effectively combine for DSC cosensitization. This chemical derivation capitalizes on the desirable optical properties of the parent dyes **1**−**7** which have led to their use in laser applications.

Our strategy begins with determining the crystal structures and optical absorption properties of **1**−**7**. These data enable the essential D-π-A intramolecular charge transfer (ICT) pathways in this dye series to be established, and the nature of their optical transitions to be identified. Such information serves to

Received: February 1, 2014
Revised: May 9, 2014
Published: June 3, 2014

   dx.doi.org/10.1021/jp501159g | *J. Phys. Chem. C* 2014, 118, 14082−14090

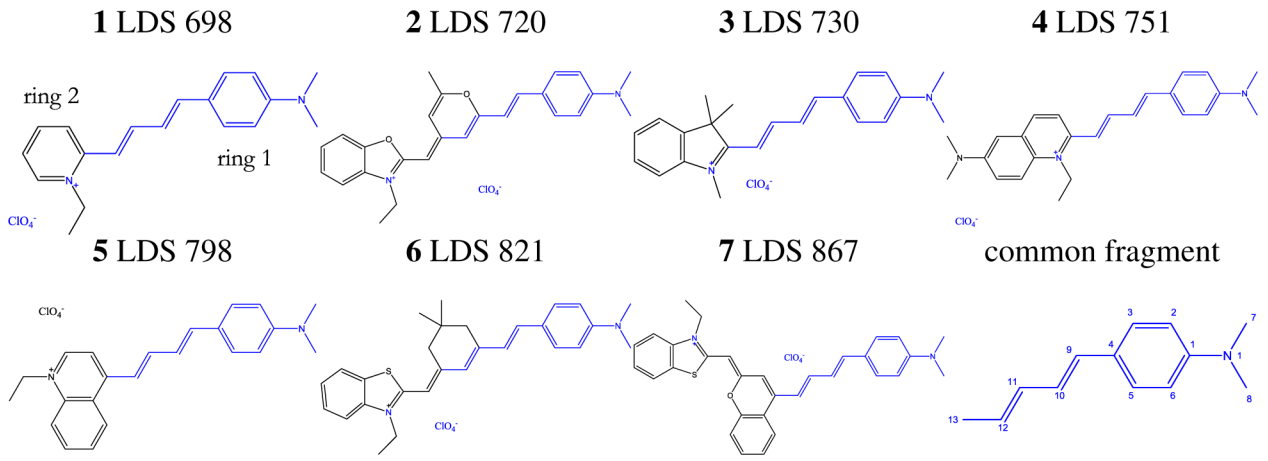

Figure 1. Chemical schematics of laser dyes **1**–**7**, along with their trade names. Common features are highlighted in blue. All dyes share an $N(CH_3)_2$ donor group attached to carbon 1, connected through a π-bridge, to a cyclic ring containing a second nitrogen atom. The bottom right schematic shows the numbering convention for the common fragment. Ring 1 refers to the benzene ring common to all dyes, and ring 2 to the ring containing the positively charged nitrogen. Dyes were supplied by the Exciton chemical company.

Table 1. Summary of Crystal Data, Data Collection, and Structure Refinement Details

	1	2[a]	3	4
chem formula	$C_{19}H_{23}ClN_2O_4$	$C_{26}H_{27}ClN_2O_6$	$C_{23}H_{27}ClN_2O_4$	$C_{25}H_{30}ClN_3O_4$
formula wt	378.84	498.95	430.92	471.97
cryst syst	triclinic	triclinic	monoclinic	monoclinic
space group	$P\bar{1}$	$P\bar{1}$	$C2/c$	$P2_1/n$
a/Å	7.662(3)	7.910(5)	30.833(5)	8.0856(13)
b/Å	11.010(4)	11.892(5)	7.2235(10)	12.518(2)
c/Å	11.473(4)	13.602(5)	22.094(4)	22.631(4)
α/deg	90.434(4)	76.675(5)	90	90
β/deg	106.459(4)	77.828(5)	119.936(2)	95.377(2)
γ/deg	103.436(5)	72.459(5)	90	90
cell vol/A^3	900.0(6)	1173.3(10)	4264.3(12)	2280.5(7)
Z	2	2	8	4
μ/mm^{-1}	0.240	0.209	0.212	0.206
F(000)	400	524	1824	1000
cryst size/mm^3	0.37 × 0.23 × 0.16	0.51 × 0.22 × 0.16	0.29 × 0.24 × 0.14	0.59 × 0.48 × 0.45
reflns collected	7406	9843	11 250	20 844
indep reflns	4005	5201	4862	5188
R_{int}	0.0367	0.0254	0.0485	0.0396
completeness to θ = 27.48°/%	97.2	96.6	99.1	99.0
restraints/params	0/238	0/320	0/276	0/303
S	1.085	1.041	1.070	1.063
R1 [$I > 2\sigma(I)$]	0.0415	0.0521	0.0456	0.0455
wR2 [$I > 2\sigma(I)$]	0.1081	0.1355	0.1169	0.1236
$\Delta\rho_{max}$, $\Delta\rho_{min}$ (e A^{-3})	0.389, −0.376	0.862, −0.674	0.322, −0.349	0.725, −0.356

[a]Counterion in **2** exhibits rotational disorder in a 3:1 component ratio.

establish the molecular design characteristics for DSC application. These crystal structures then provide a starting point for density functional theory and time-dependent density functional theory calculations on computationally designed chemical derivatives of these seven parent dyes that incorporate an anchoring group necessary for adsorption onto the DSC semiconductor electrode. Based on energetic and geometric considerations, a pair of these modified dyes is proposed for DSC cosensitization.

METHODS

Single Crystal X-ray Diffraction. **1**–**7** were supplied by Exciton and crystallized without further purification. Crystals were grown by solvent evaporation at room temperature in methanol for **1** and **3**, dichloromethane for **2**, **4**, **5**, and **6**, and acetone for **7**. Single crystal data were collected at 120 K on a Rigaku Saturn 724+ CCD diffractometer with a molybdenum X-ray source (wavelength 0.71073 Å), SHINE Optics, and an Oxford Cryostreams CryostreamPlus open-flow nitrogen cooling system. Cell refinement, data collection, and data reduction used Rigaku CrystalClear-SM Expert 2.0 software.[5] An absorption correction was implemented with ABSCOR.[6] Structures were solved by direct methods and refined by full-matrix least-squares methods on F^2 values, using SHELXS.[7] Hydrogen atoms were positioned geometrically, and refined as

dx.doi.org/10.1021/jp501159g | J. Phys. Chem. C 2014, 118, 14082–14090

riding on their parent atoms. A summary of crystal data, data collection, and refinement details is given in Tables 1 and 2.

Table 2. Summary of Crystal Data, Data Collection, and Structure Refinement Details

	5	6[a]	7[a]
chem formula	$C_{23}H_{25}ClN_2O_4$	$C_{28}H_{33}ClN_2O_4S\cdot 0.5(CCl_2)$	$C_{31}H_{29}ClN_2O_5S\cdot 0.25(C_2O_{0.5})$
formula wt	428.90	570.53	583.08
cryst syst	monoclinic	triclinic	triclinic
space group	$P2_1/n$	$P\bar{1}$	$P\bar{1}$
a/Å	11.101(3)	9.770(4),	8.027(10)
b/Å	16.452(4)	12.728(5)	11.283(13)
c/Å	12.347(4)	13.240(5)	17.69(2)
α/deg	90	99.575(3)	92.665(19)
β/deg	108.375(4)	111.360(2)	102.552(17)
γ/deg	90	105.870(4)	99.03(2)
cell vol/A^3	2140.0(10)	1408.4(10)	1539(3)
Z	4	2	2
μ/mm^{-1}	0.211	0.342	0.233
F(000)	904	600	610
cryst size/mm^3	0.6 × 0.37 × 0.24	0.36 × 0.26 × 0.17	0.31 × 0.22 × 0.19
reflns collected	17 792	10 558	10 289
indep reflns	4899	6233	5359
R_{int}	0.0412	0.0393	0.0468
completeness to θ = 27.48/%	99.8	96.5	98.4
rstraints/params	0/274	0/355	2/391
S	1.082	1.047	1.061
R1 [$I > 2\sigma(I)$]	0.0496	0.0464	0.072
w$R2$ [$I > 2\sigma(I)$]	0.1255	0.123	0.1979
$\Delta\rho_{max}$, $\Delta\rho_{min}$ (e A^{-3})	0.478, −0.370	0.547, −0.34	0.657, −0.361

[a] **6** and **7** contain disordered dichloromethane and disordered acetone in 2:1 and 4:1 dye:solvent ratios, respectively.

UV−Vis Absorption Spectroscopy. Measurements on **1**−**7** were taken in methanol, using a Hewlett-Packard G1103A spectrophotometer. Peak molar extinction coefficients, ε, were determined by measuring peak absorbances for five different concentrations. Molar extinction coefficients were then extracted from the gradients of the graphs of peak absorbance versus concentration. ε for **1** was taken from the literature.[8]

DFT and TDDFT Calculations. The seven determined crystal structures were used as initial input geometries for DFT and TDDFT calculations to develop an effective computational strategy for the subsequent molecular engineering. Therein, structural, electronic, and optical properties were calculated in order to characterize the nature of photoexcitation.

Ground-state geometries were optimized by DFT, using the B3LYP functional,[9] and a 6-31++G(d,p) basis set within the Gaussian 09 package,[10] and solvent effects were included through the polarizable continuum model (PCM).[11,12] Analytic frequency calculations were performed to ensure that the lowest vibrational frequencies were real, and an energy minimum was reached. The optimized geometries were found to be similar to those determined from the crystal structures.

Low lying vertical excitation energies were determined by TDDFT calculations using the B3LYP optimized geometries,[13] and the PCM was used to model the solvent.[11,12] The model simulated methanol solvent so that calculations could be compared with experiment, and excitation energies were calculated using nonequilibrium solvation, in which there is electronic polarization of the solvent, but no nuclear reorganization.[14]

Since TDDFT with standard local exchange-correlation kernels significantly underestimates excitations with significant charge transfer, that are characteristic of organic DSC dyes,[15] a range of functionals: B3LYP, CAM-B3LYP, M062X, and PBE1PBE, were each tested for their accuracy in calculating low-lying excitation energies using a 6-31++G(d,p) basis set (see Supporting Information). PBE1PBE offered the lowest average absolute deviation from experiment of 0.10 eV and was therefore used for all the dyes discussed. The accuracy of this functional can be explained by the intermediate-to-high overlap between the occupied and unoccupied Kohn−Sham orbitals involved in the excitations[15] (full details are contained in the Supporting Information).

RESULTS AND DISCUSSION

Establishing DSC Design Prerequisites. Figure 2 shows the molecular structures of **1**−**7** determined by X-ray diffraction. Analysis of their bond lengths and angles enables the identification of the donor (D), acceptor (A), and π-conjugated bridging constituents, that afford the D-π-A intramolecular charge transfer (ICT) pathway through each molecule. Defining such pathways, especially the substitution point for the acceptor group, is a prerequisite for designing DSC dyes with suitable anchoring groups.[17,18] Owing to the molecular fragment that is common to all seven structures (see Figure 1), the donor, D = NMe_2, and at least the initial part of the π-conjugated pathway is anticipated. The NMe_2 donor attributes are confirmed by the pronounced π-conjugated character of its C1−N1 bond (1.366(2)−1.378(5) Å); this is not much longer than that in one of the most classically strong D-π-A molecules, *p*-nitroaniline (1.355 Å)[19] or its more chemically comparable dimethylaniline derivative (1.358 Å).[20] The electron-donating nature of the C1−N1 bond influences the distinct para-quinoidal nature of the vicinal ring, as indicated by the consistently shorter C2−C3 (1.376(2)−1.386(3) Å) and C5−C6 bonds (1.372(2)−1.391(5) Å) relative to the other bond lengths in ring 1 which have an average value of $\bar{x}$ = 1.41(1) Å across the seven structures. The alternating double- and single-bonding pattern in the continuing olefinic chain, as represented in Figure 1, is in agreement with the corresponding crystallographic bond analysis. This is perhaps surprising given the pronounced quinoidal character of the ring; this means that there is a one-bond (C4−C9) slip in the otherwise dominant double−single bonding alternation. The π-conjugation that binds these rings and olefinic molecular fragments nonetheless turns out to be sufficiently strong to maintain an effective ICT pathway between them, as evidenced by the near-perfect plane that these two fragments form together.

The ICT pathway extends beyond the common molecular fragment. In the case of **1**, **3**, **4**, and **5**, the olefinic terminus of the common fragment directly adjoins a C═N$^+$ bond, while a −C═C− unit separates the common olefinic fragment, and a C═N$^+$ bond in **2** and **6**. As for **7**, two −C═C− units separate such moieties. In all cases, a continuing alternate double−single π-bonding pattern is observed up to the site of formal positive charge, N$^+$ (N2), albeit becoming a little blurred when passing through the prevailing formally aromatic rings, as one might expect. The ICT pathway appears to terminate in proximity to N2, although it is difficult to locate precisely owing to the

dx.doi.org/10.1021/jp501159g | J. Phys. Chem. C 2014, 118, 14082−14090

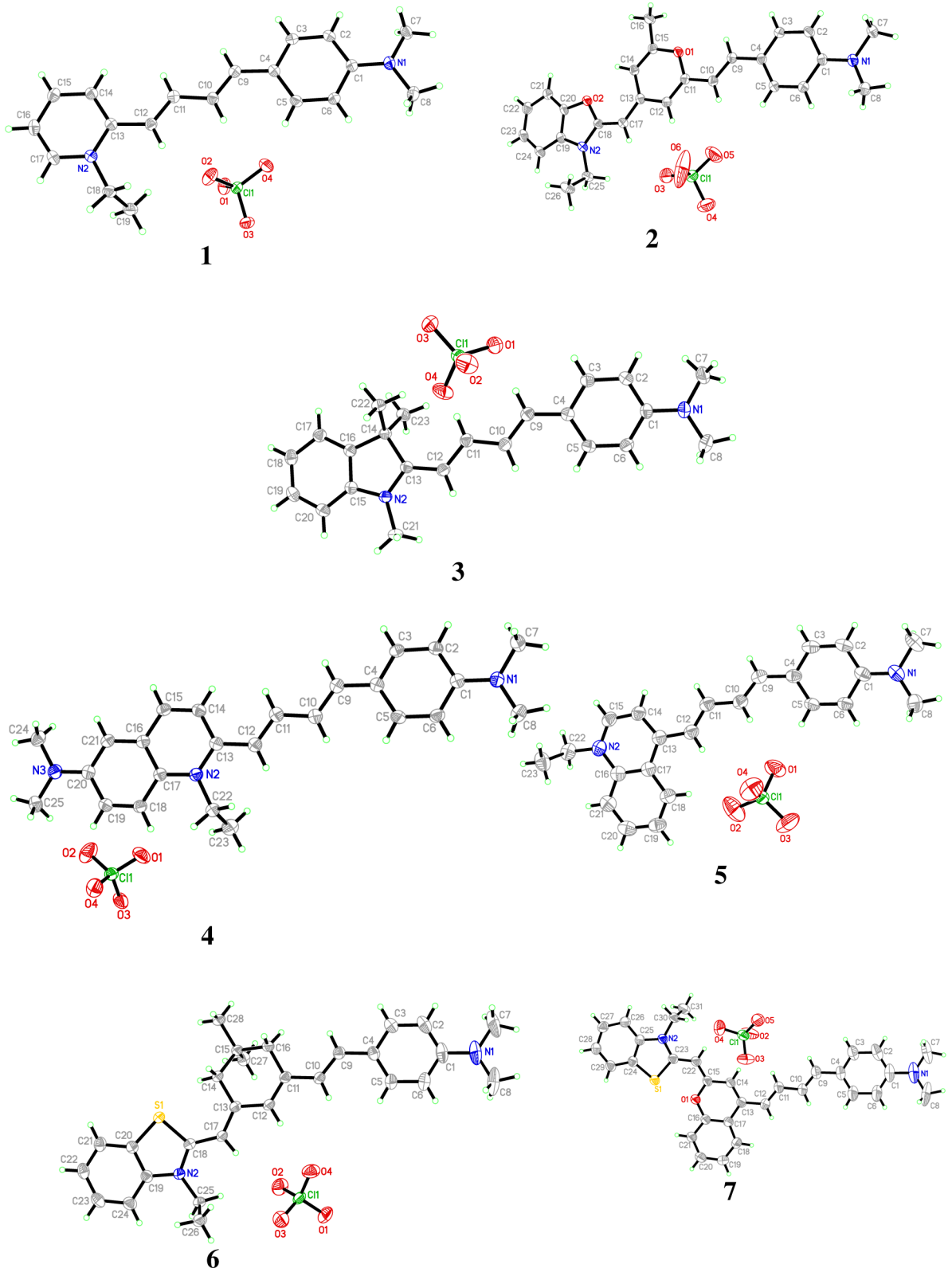

Figure 2. 50% probability anisotropic displacement parameter (ADP) plots for the labeled crystal structures. Crystal data for **1** were previously measured, with its structure determined at 296 K;[16] data were remeasured here, but at 120 K, to enable a common comparison of all structures.

blurring of a definitive alternating bonding pattern. In the absence of further information, it is possible that other heteroatoms (S and O) in the same region as N2 may also influence the ICT path at this point, where they are present (**2**, **6**, and **7**). What does seem apparent, however, is that wherever a benzenoid ring resides beyond N2, relative to this ICT path trajectory, such rings all exhibit highly aromatic character. Such delocalization implies that these rings behave as units of charge-transfer inhibition. That said, such rings could be influential on steric grounds, controlling the crystal packing in the solid state

dx.doi.org/10.1021/jp501159g | J. Phys. Chem. C 2014, 118, 14082−14090

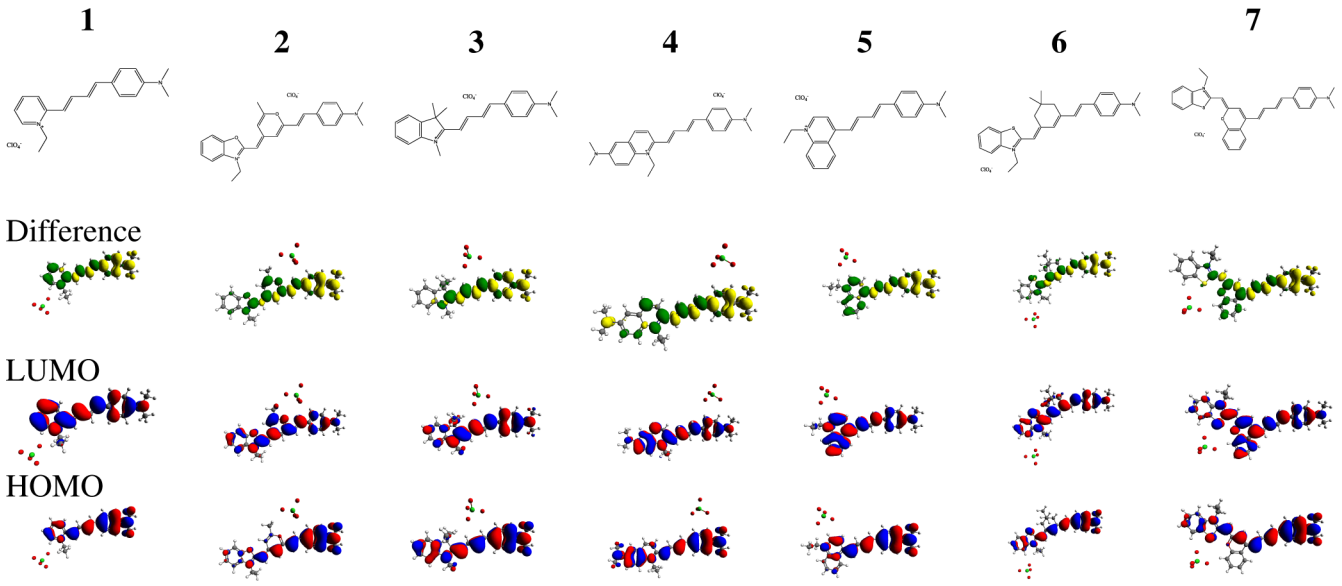

Figure 3. HOMO, LUMO, and difference-density isoplots, and chemical schematic for dyes **1**−**7**. For the HOMO/LUMO plots, the isovalue is 0.02. Difference plots are created from squaring the LUMO/HOMO isoplots and subtracting them, representing changes in electron density. Yellow represents a negative isovalue, where electron density has decreased in going from HOMO to LUMO, green a positive isovalue, where it has increased. The isovalue for the difference plot has been arbitrarily chosen to be 0.001.

or, once functionalized with a suitable anchor, physically restricting the anchoring configuration of the dye molecule on the TiO_2 surface in a DSC working electrode or, if oriented on the other side of the anchoring point, provide a physical blocking moiety to offset undesirable electron recombination effects. From this bond-length analysis, the ICT pathway can therefore be tentatively be assigned as a "push−pull" traversal from NMe_2 to N2.

In order to confirm that the ICT terminus lies in the region of N2, the changes in molecular orbital populations associated with optical absorption were approximated using DFT calculations.[13,21] Figure 3 displays the resultant HOMO, LUMO, and difference-density isoplots, where the difference plots were generated by subtracting the square of the HOMO plots from the square of the LUMO plots since the TDDFT calculations indicated the HOMO−LUMO transition as predominant. The corresponding isosurfaces represent the changes in electron density between HOMO and LUMO levels: yellow representing a negative isovalue, where electron density has decreased in the HOMO-to-LUMO transition; green a positive isovalue, where it has increased.

Figure 3 highlights a common feature of all seven dyes: depletion of electron density from N1 and part of ring 1 in going from HOMO to LUMO, revealed by the yellow surfaces around N1 in the difference plots, and increasing electron density on N2 or nearby group, highlighted by the green surfaces on or around N2. This corroborates the notion that photoexcitation causes charge transfer from a donor group around N1, through the π-bridge to an acceptor group, increasing electron density toward ring 2. For **2** and **7**, these plots also suggest that a conjugated ring in the π-bridge acts to filter charge, reducing charge transfer to ring 2.

Figure 4 shows the normalized experimental UV−vis spectra of dyes **1**−**7**. (Extracted absorption properties are summarized in Table 1 of the Supporting Information.) Each dye shows a well-defined absorption band with peak absorption wavelengths ranging from 486 to 609 nm, and extinction coefficients in the range $(4.2–7.2) \times 10^4$ M^{-1} cm^{-1}, which exceed the *N3* dye by

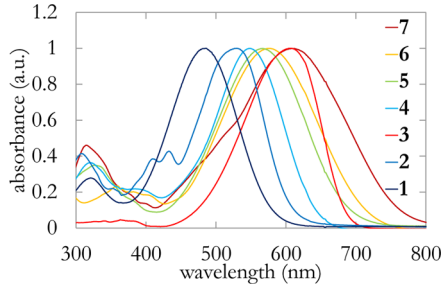

Figure 4. Overlaid normalized absorption spectra for dyes **1**−**7**.

approximately three to five times,[2] highlighting their potential for DSC applications.

The identification of donor/acceptor groups, ICT, and optical transitions in these seven parent dyes provides the foundation for designing new sensitizer derivatives. Using the insights gained from **1**−**7**, derivatives can be tailored with appropriate charge-transfer character, effective placement of the anchor group, and donor/acceptor modifications that produce the desired spectral coverage.

Designing DSC Dyes Based on 1−7. To operate in a DSC, an anchor group such as COOH must be present on the dye molecule to enable adsorption to the semiconductor electrode (typically TiO_2 nanoparticles). No such group is present in **1**−**7**. Consequently, 22 modified dyes were created computationally by substituting a carboxylic acid group at various positions in the parent dyes **1**−**7**. The selection of the modified dyes can be summarized by the following simple design concepts: the anchor group should be positioned close to the acceptor moeity (either near N2 or, in the case of **7**, on the aromatic fragment connected to the π-bridge) to enable effective charge transfer to the semiconductor electrode, and its position should minimize unfavorable molecular distortions which disrupt favorable charge transfer, while maximizing the net charge transfer to the anchor group, up to a point. It has in fact been recently demonstrated that a D-π_1-A-π_2-Ads

dx.doi.org/10.1021/jp501159g | J. Phys. Chem. C 2014, 118, 14082−14090

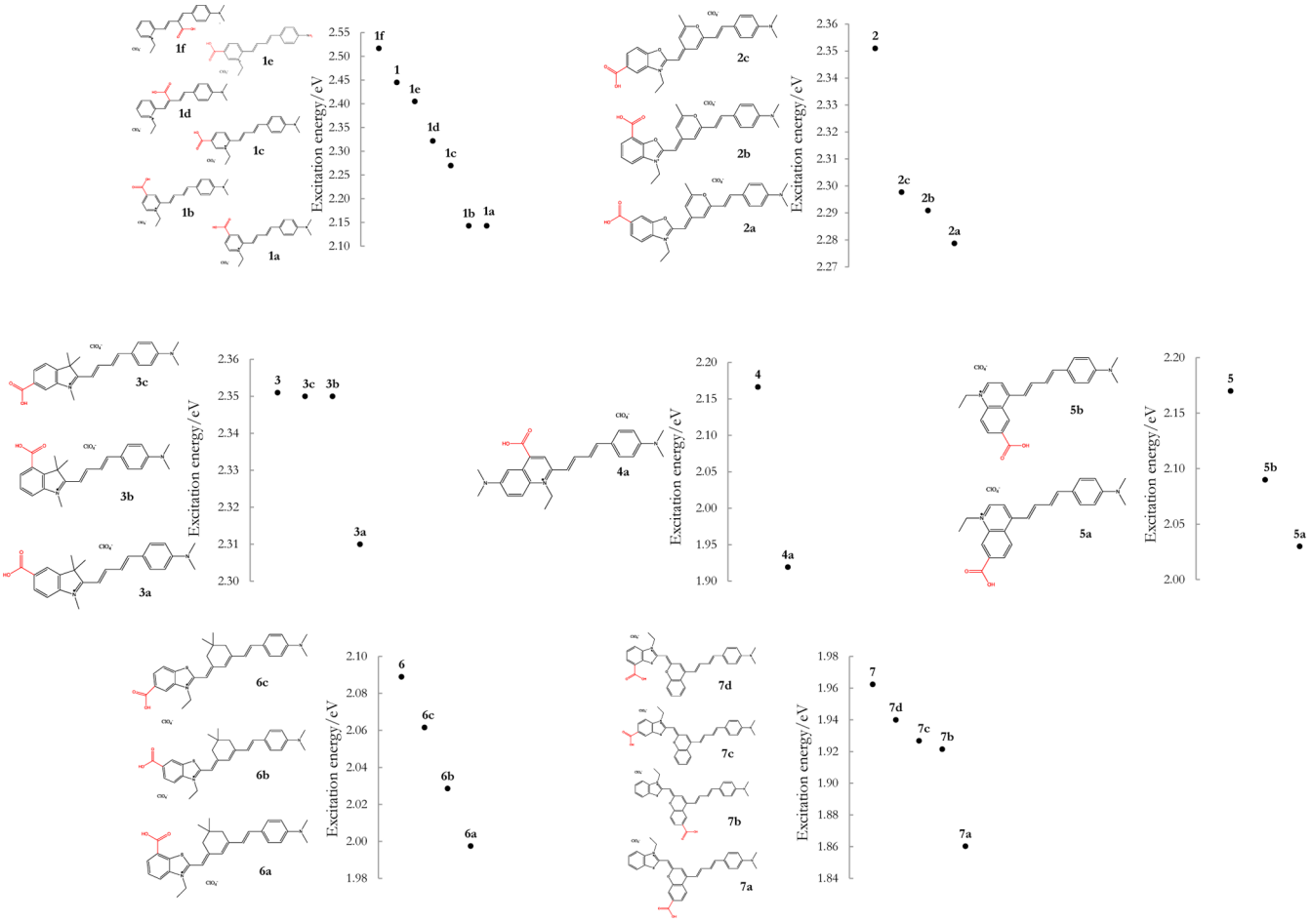

Figure 5. Designed dyes with carboxylic acid anchor group. The number associated with each dye refers to the parent dye on which it is based.

molecular architecture (where π_2 is a phenyl ring and Ads is a COOH group) can afford a more than six times improvement in DSC performance in dyes compared to their D-π-A analogue, where A = Ads.[22] This separation of A and Ads via a phenyl ring is thought to provide sufficient aromatic ring stabilization to inhibit the back-transfer of electronic charge from TiO_2 to A, thereby circumventing undesirable electron recombination.[23] It is encouraging that the crystal structures of this series of dyes demonstrate the same aromatic stabilization of the phenyl rings beyond their ICT pathway. The provident design of dyes bearing COOH substitution upon these rings which separate A and Ads by a phenyl ring therefore attests to their potential ability to similarly inhibit unfavorable electron back-transfer.

The substitution point within the ring was also varied since it stands to affect this charge-transfer inhibition property significantly: only ortho- and para-COOH substitution will permit competition between aromatic and quinoidal resonance states; it is impossible to create a quinoidal resonance structure via meta-substitution where COOH is the charge-transfer recipient while retaining a neutrally charged ring. The effect of positioning the anchor within the olefinic π-bridge of **1** and the fused rings that precede A in **7** was also explored; this design enables the COOH group to somewhat extrude from the molecule at such substitution points, which will expose it to the TiO_2 surface less hindered from the steric bulk of the molecular dye. In addition, a modified donor group was used to blue-shift absorption, and extend spectral coverage. DFT/TDDFT calculations were performed to characterize the effect of introducing this anchor group on excitation energy, ICT characteristics, and molecular geometry.

Screening Based on Excitation Energies. Figure 5 shows the chemical schematics for the designed dyes, along with their calculated excitation energies, with each set presented in order of decreasing excitation energy. Dye designs based on **1** and **7** show the greatest complementary absorption energy span. All things being equal, this pair would therefore offer the best panchromatic response if employed together for DSC cosensitization. In the absence of other considerations, derivatives of **1** and **7** would thus appear to have the most potential for device application.

1b and **1a** were used to test the effect of the two possible (180°-separated) planar-COOH conformations of the anchor at a given substitution point. Their HOMOs and excitation energies were indistinguishable, suggesting that initial orientation was not critical. Excitation energies for **1b** and **1c** were red-shifted by 0.31 and 0.18 eV, with corresponding isoplots suggesting successful charge transfer to the anchor. **7a** showed the largest red-shift (0.10 eV) for the various modifications of the parent dye **7**, with the greatest charge transfer to the anchor (Figure 7b). Red-shifts of less than 0.04 eV were found for **7c** and **7d**, with minor charge transfer to the anchor; as suggested by Figure 3, the charge transfer occurs mainly to the fused rings in the π-bridge.

In general, insertion of the anchor group was found to result in a red-shift in peak absorption energy compared to the parent

dx.doi.org/10.1021/jp501159g | J. Phys. Chem. C 2014, 118, 14082−14090

dye, with increasing red-shift according to a greater degree of charge transfer to the anchor. This is a beneficial result for DSC dyes for which one of the problems has been retaining absorption in the near-infrared upon adsorption to the semiconductor. In cases such as **1f**, insertion of the anchor group resulted in significant distortion of the molecular geometry, resulting in poor charge-transfer characteristics, and a resultant weak red- or even blue-shift in excitation energy compared to the parent dye. Designs with these distortions were ruled out for prospective cosensitization.

Due to the decreased excitation energies on addition of the anchor group, and the need for complementary absorption spectra for cosensitization, **1e** was designed with a reduced donor strength (D = NH_2) to produce a blue-shift relative to **1c** (D = NMe_2).

Screening Based on LUMO Energies. Injection from dye to semiconductor requires the energy level of a dye LUMO to be above that of the semiconductor conduction band. The energy difference between the dye LUMO level and TiO_2 conduction band is a key factor in determining the injection rate, and hence the photocurrent.[24] Calculated LUMO levels can therefore act as a screening tool for new sensitizers. If this energy difference is too low, then a dye can be ruled out. A computationally efficient approximation to the LUMO level is to add the TDDFT vertical excitation energy to the dye HOMO level.[25]

In a DSC, interactions due to adsorption onto the semiconductor will shift the energy levels of the combined dye−nanoparticle system compared to the noninteracting case. However, alignment of energy levels of the noninteracting species has offered a good approximation for interacting systems[25,26] and provides an efficient screening tool to assess whether new dyes would be suitable for DSC applications.[27]

Figure 6 shows the HOMO and LUMO energies for a selection of the designed dyes for which steric considerations

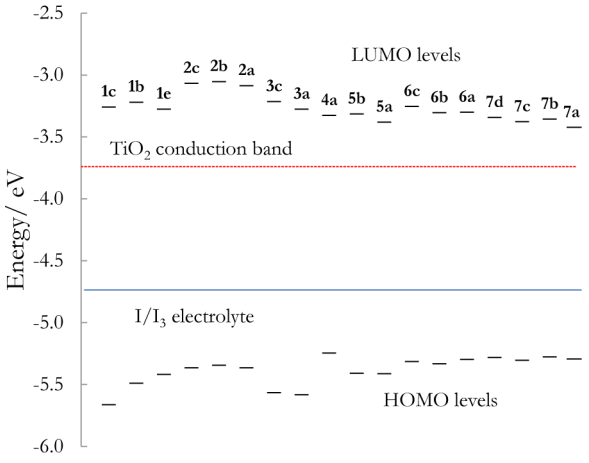

Figure 6. Calculated HOMO and LUMO energies (versus vacuum) for selected designed dyes, with TiO_2 anatase (101) conduction band (red dotted line), and the I^-/I_3^- electrolyte redox potential for comparison.[28] The calculated LUMOs lie at least 0.32 eV above the conduction band. The number labels refer to the parent dye.

did not rule out by disrupting ICT pathways, along with the conduction band edge of the TiO_2 anatase (101) surface, taken as −3.74 eV[29] (the red line in Figure 6), and the I^-/I_3^- electrolyte redox potential.[28]

LUMOs of all dyes are found to lie above the TiO_2 conduction band, with maximum and minimum deviations of 0.69 and 0.32 eV for **2b** and **7a**. HOMOs were found to below the iodide/triiodide redox potential, taken as −4.85 eV,[28] with maximum and minimum values of −5.24 and −5.58 eV, for **4a** and **1e**.

Forming a DSC Cosensitization Strategy. Based on the calculated excitation energies, energy-level positioning, and charge-transfer characteristics, we propose **7a** and **1e** as possible dyes for cosensitization. This pairing offers the following: separated calculated absorption maxima at 666 and 516 nm, to provide the broadest spectral coverage; isoplots showing successful charge transfer to the anchor (Figure 7b); LUMO energy levels above the TiO_2 conduction band; HOMO energy levels below the electrolyte redox potential; geometrical positioning of the anchor allowing exposure to the semiconductor; and chemical similarity to minimize detrimental interactions. Furthermore, high molecular extinction coefficients of the parent dyes indicate their promise.

The UV−vis spectra for these two selected dyes were simulated by convolving the four lowest lying optical excitations of each dye with a Gaussian energy profile with a full-width-half-maximum equal to that of the parent dye. These spectra are shown in Figure 7 along with their superposition, and the standard AM 1.5 solar spectrum for comparison. The absorption has been assumed to be additive, which has been found in previous successful cosensitization strategies, where detrimental dye···dye interactions were minimized.[30] The superposition of the two defined absorption bands results in optical absorption over the entire visible range, with extension into the infrared, highlighting the potential for cosensitization of these dyes, and the benefits for panchromatic spectral coverage. We note that while obtaining broad spectral coverage is an important factor in determining the overall power conversion efficiency of a DSC, this will also be influenced by electron injection into the semiconductor and transport to the electrodes which must compete with unwanted recombination. Charge transfer between cosensitizers may also be problematic, but as demonstrated by Jeong et al.,[31] this may be reduced by spatial separation of the two chromophores.

Finally, it is interesting to note that these two selected cosensitizers appear to conform well to the recently proposed superior D-π-A-π-Ads molecular architecture for DSC dyes.[22] Based on their difference density isoplots, both **1e** and **7a** show a strong ICT pathway from the donor out to the region of N2, i.e., good D-π-A characteristics. Meanwhile, the π in the π-Ads unit comprises a phenyl group that carries a para-substituted COOH anchor, and this moiety displays almost wholly positive isosurfaces; this suggests that it acts a sink of electron density, inhibiting electronic charge back-transfer to the D-π-A pathway. The fact that these computations have naturally selected cosensitizers whose molecular architecture bears a para-aromatic spacer between A and Ads attests to its claimed importance in DSC dye design.

■ CONCLUSIONS

In summary, a strategy for materials discovery of high extinction organic dyes suitable for cosensitization in DSCs has been implemented. Seven crystal structures of organic dyes without the necessary anchor group for DSC applications have been determined, along with their UV−vis absorption spectra and extinction coefficients, forming the basis for DFT/TDDFT calculations on 22 modified dyes which do include a suitable anchor.

dx.doi.org/10.1021/jp501159g | J. Phys. Chem. C 2014, 118, 14082−14090

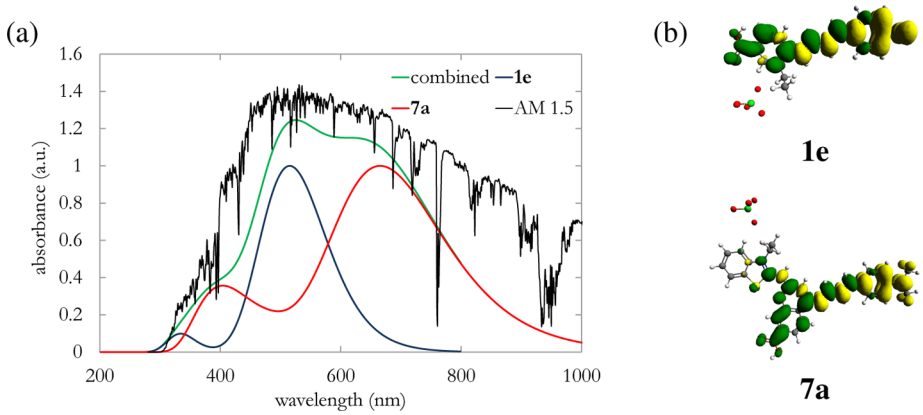

Figure 7. (a) Simulated absorption spectra for **1e** and **7a**, along with their superposition, and the standard AM 1.5 solar spectrum for comparison. The heights of the spectra are arbitrary and have been offset for clarity. The superposition is calculated from the addition of the normalized spectra of the two dyes. (b) Difference plots for **1e** and **7a** showing the successful charge transfer to the anchor group which was associated with a red-shift in peak absorption energy compared to the parent dye.

Molecular geometry, HOMO/LUMO positioning, excitation energies, and charge-transfer characteristics have been used as screening tools to predict the suitability of the modified dyes for DSC use. On the basis of these criteria, a possible cosensitization strategy has been suggested, using two of the designed dyes, and their UV−vis absorption spectra have been simulated.

Experimental validation of these predictions will enable this design route to be further tested, and allow further families of DSC dyes to be predicted.

■ ASSOCIATED CONTENT

Supporting Information

Further computational detail. This material is available free of charge via the Internet at http://pubs.acs.org.

■ AUTHOR INFORMATION

Corresponding Author

*E-mail: jmc61@cam.ac.uk.

Notes

The authors declare no competing financial interest.

■ ACKNOWLEDGMENTS

S.L.B. thanks Jignesh Radia and Kian Sing Low for useful discussions. J.M.C. acknowledges the Royal Society for a University Research Fellowship, the Fulbright Commission for a UK-US Fulbright Scholar Award, the ICAM Branches Cost Sharing Fund, and the Bragg Institute, ANSTO, Australia, for funding (for P.G.W.). The authors thank the EPSRC UK National Service for Computational Chemistry Software (NSCCS), based at Imperial College London, and acknowledge contributions from its staff in supporting this work. S.M. is grateful to King's College, University of Cambridge, U.K., and the EPSRC (Grant EP/P505445/1) for PhD funding. X.L. is indebted to the Singapore Economic Development Board for a Clean Energy Scholarship. Work done at Argonne National Laboratory (J.M.C.) was supported by DOE Office of Science, Office of Basic Energy Sciences, under Contract No. DE-AC02-06CH11357.

■ REFERENCES

(1) O'Regan, B.; Gratzel, M. A Low-Cost, High-Efficiency Solar Cell Based on Dye-Sensitized Colloidal TiO2 Films. *Nature* **1991**, *353*, 737−740.
(2) Chen, Y.; Zeng, Z.; Li, C.; Wang, W. Highly Efficient Co-sensitization of Nanocrystalline TiO2 Electrodes with Plural Organic Dyes. *New J. Chem.* **2005**, *29*, 773−776.
(3) Ogura, R. Y.; Nakane, S.; Morooka, M.; Orihashi, M.; Suzuki, Y.; Noda, K. High-Performance Dye-Sensitized Solar Cell with a Multiple Dye System. *Appl. Phys. Lett.* **2009**, *94*, 073308.
(4) Robertson, N. Catching the Rainbow: Light Harvesting in Dye-Sensitized Solar Cells. *Angew. Chem., Int. Ed.* **2008**, *47*, 1012−1014.
(5) Rigaku. *CrystalClear SM Expert and CrystalStructure*, 2009.
(6) Higashi, T. *ABSCOR*; Rigaku Corporation: 1995.
(7) Sheldrick, G. M. Found. Crystallogr. *Acta Crystallogr., Sect. A: Found. Crystallogr.* **2008**, 112−122.
(8) Exciton, LDS 698 data sheet.
(9) Becke, A. D. A New Mixing of Hartree Fock and Local Density Functional Theories. *J. Chem. Phys.* **1993**, *98*, 1372−1377.
(10) Frisch, M. J.; et al. *Gaussian 09*, Gaussian, Inc.: Wallingford, CT, 2009.
(11) Yao, H.; Yamashita, M.; Kimura, K. Organic Styryl Dye Nanoparticles: Synthesis and Unique Spectroscopic Properties. *Langmuir* **2009**, *25*, 1131−1137.
(12) Fantacci, S.; De Angelis, F.; Selloni, A. Absorption Spectrum and Solvatochromism of the [Ru(4,4′-COOH-2,2′-bpy)2(NCS)2] Molecular Dye by Time Dependent Density Functional Theory. *J. Am. Chem. Soc.* **2003**, *125*, 4381−4387.
(13) Pastore, M.; Mosconi, E.; Angelis, F. D.; Gra, M. A Computational Investigation of Organic Dyes for Dye-Sensitized Solar Cells: Benchmark, Strategies, and Open Issues. *J. Phys. Chem. C* **2010**, *114*, 7205−7212.
(14) Tomasi, J.; Mennucci, B.; Cammi, R. Quantum Mechanical Continuum Solvation Models. *Chem. Rev.* **2005**, *105*, 2999−3093.
(15) Peach, M. J. G.; Benfield, P.; Helgaker, T.; Tozer, D. J. Excitation Energies in Density Functional Theory: an Evaluation and a Diagnostic Test. *J. Chem. Phys.* **2008**, *128*, 044118.
(16) Jasinski, J. P.; Jasinski, J. M.; Crosby, D. J. 2-{4-[4-(Dimethylamino)phenyl]-1,3-butadienyl}-1-ethylpyridinium perchlorate. *Acta Crystallogr., Sect. E: Struct. Rep. Online* **2002**, *58*, 1283−1284.
(17) Liu, X.; Cole, J. M.; Waddell, P. G.; Lin, T.-C.; Radia, J.; Zeidler, A. Molecular origins of optoelectronic properties in coumarin dyes: toward designer solar cell and laser applications. *J. Phys. Chem. A* **2012**, *116*, 727−37.
(18) Zhang, L.; Cole, J.; Waddell, P.; Low, K. S.; Liu, X. Relating Electron Donor and Carboxylic Acid Anchoring Substitution Effects in

Azo Dyes to Dye-Sensitized Solar Cell Performance. *ACS Sustainable Chem. Eng.* **2013**, *1*, 1440−1452.
(19) Tonogaki, M.; Kawata, T.; Ohba, S.; Iwata, Y.; Shibuya, I. Electron-Density Distribution in Crystals of p-Nitrobenzene Derivatives. *Acta Crystallogr., Sect. B: Struct. Sci.* **1993**, *49*, 1031−1039.
(20) Borbulevych, O.; Clark, R.; Romero, A. Experimental and Theoretical Study of the Structure of N,N-dimethyl-4-Nitroaniline Derivatives as Model Compounds for Non-linear Optical Organic Materials. *J. Mol. Struct.* **2002**, *604*, 73−86.
(21) Stowasser, R.; Hoffmann, R. What Do the Kohn-Sham Orbitals and Eigenvalues Mean ? *J. Am. Chem. Soc.* **1999**, *121*, 3414−3420.
(22) Haid, S.; Marszalek, M.; Mishra, A.; Wielopolski, M.; Teuscher, J.; Moser, J.-E.; Humphry- Baker, R.; Zakeeruddin, S. M.; Grätzel, M.; Bäuerle, P. Significant Improvement of Dye-Sensitized Solar Cell Performance by Small Structural Modification in π-Conjugated Donor-Acceptor Dyes. *Adv. Funct. Mater.* **2012**, *22*, 1291−1302.
(23) Kim, B.-G.; Chung, K.; Kim, J. Molecular Design Principle of All-Organic Dyes for Dyesensitized Solar Cells. *Chemistry* **2013**, *19*, 5220−5230.
(24) Asbury, J. B.; Anderson, N. A.; Hao, E.; Ai, X.; Lian, T. Parameters Affecting Electron Injection Dynamics from Ruthenium Dyes to Titanium Dioxide Nanocrystalline Thin Film. *J. Phys. Chem. B* **2003**, *3*, 7376−7386.
(25) De Angelis, F.; Fantacci, S.; Selloni, A. Alignment of the Dye's Molecular Levels with the TiO2 Band Edges in Dye-sensitized Solar Cells: a DFT-TDDFT Study. *Nanotechnology* **2008**, *19*, 424002.
(26) Le Bahers, T.; Pauporté, T.; Scalmani, G.; Adamo, C.; Ciofini, I. A TD-DFT Investigation of Ground and Excited State Properties in Indoline Dyes Used for Dye-Sensitized Solar Cells. *Phys. Chem. Chem. Phys.* **2009**, *11*, 11276−11284.
(27) Nazeeruddin, M. K.; De Angelis, F.; Fantacci, S.; Selloni, A.; Viscardi, G.; Liska, P.; Ito, S.; Takeru, B.; Grätzel, M. Combined Experimental and DFT-TDDFT Computational Study of Photoelectrochemical Cell Ruthenium Sensitizers. *J. Am. Chem. Soc.* **2005**, *127*, 16835−16847.
(28) Nattestad, A.; Ferguson, M.; Kerr, R.; Cheng, Y.-B.; Bach, U. Dye-sensitized Nickel(II)Oxide Photocathodes for Tandem Solar Cell Applications. *Nanotechnology* **2008**, *19*, 295304.
(29) Labat, F.; Adamo, C. Bi-isonicotinic Acid on Anatase (101): Insights from Theory. *J. Phys. Chem. C* **2007**, *111*, 15034−15042.
(30) Grätzel, M. Dye-sensitized Solar Cells. *J. Photochem. Photobiol., C* **2003**, *4*, 145−153.
(31) Jeong, N. C.; Son, H.-J.; Prasittichai, C.; Lee, C. Y.; Jensen, R. a.; Farha, O. K.; Hupp, J. T. Effective panchromatic sensitization of electrochemical solar cells: strategy and organizational rules for spatial separation of complementary light harvesters on high-area photoelectrodes. *J. Am. Chem. Soc.* **2012**, *134*, 19820−19827.